

## Synthesis and antibacterial activity of transition metal (Ni/Mn) co-doped TiO<sub>2</sub> nanophotocatalyst on different pathogens under visible light irradiation

Sankara Rao Meditana<sup>1,2,a</sup>, Siva Rao Tirukkovalluri<sup>2,b</sup>, Imandi Manga Raju<sup>2,c</sup>

<sup>1</sup>Government Degree College, Puttur, Chittoor, Andhra Pradesh – 517583, India

<sup>2</sup>Andhra University, Visakhapatnam, Andhra Pradesh – 530003, India

<sup>a</sup>sraom90@gmail.com, <sup>b</sup>sivaraou@gmail.com, <sup>c</sup>mangorchem@gmail.com

Corresponding author: Sankara Rao Meditana, sraom90@gmail.com

**ABSTRACT** Visible light driven photocatalytically active mesoporous nanomaterials plays an indispensable role for antibacterial activity in low light applications. In this work, nanomaterials were handily prepared by varying the dopant concentrations from 0.25 to 1.0 Wt % using sol-gel method. All the prepared samples were characterized by Powdered X-ray diffraction (XRD), Scanning electron microscope-energy dispersive X-ray spectroscopy (SEM-EDS), Fourier transform infrared spectroscopy (FTIR), Ultraviolet-visible diffuse reflectance spectroscopy (UV/Vis-DRS), Transmission electron microscopy (TEM) and Brauner–Emmett–Teller (BET). The characterization results revealed that a photocatalytically active phase i.e.; anatase and rutile mixed phase was observed for co-doped catalyst samples. Due to substitutional doping of Mn and Ni by replacing Ti, the frequency shift of Ti–O–Ti in the catalyst samples was observed by FTIR. Further the catalyst shows rough morphology, irregular particle shape with less particle size having high surface area, and reduced band gap energy. The photocatalytically active materials antibacterial activity was discerned by using *Sphingomonas paucimobilis* and *Pseudomonas fluorescense*. The result of antibacterial activity shows that among all nanocatalysts, NMT2 catalyst shows optimum zone of inhibition at  $25.1 \pm 0.2$  mm for *Sphingomonas paucimobilis* and  $18.1 \pm 0.2$  mm for *Pseudomonas fluorescense* compared to standard (chloramphenicol) value at  $24.1 \pm 0.1$  mm and  $23.1 \pm 0.05$  mm at 100  $\mu\text{g}/\text{mL}$  respectively.

**KEYWORDS** nanomaterials, photocatalysis, Ni/Mn–TiO<sub>2</sub>, antibacterial activity, agar-well diffusion method

**FOR CITATION** Meditana S.R., Tirukkovalluri S.R., Raju I.M. Synthesis and antibacterial activity of transition metal (Ni/Mn) co-doped TiO<sub>2</sub> nanophotocatalyst on different pathogens under visible light irradiation. *Nanosystems: Phys. Chem. Math.*, 2022, **13** (1), 104–114.

### 1. Introduction

TiO<sub>2</sub> is an acquainted photocatalyst with non-toxicity, inexpensive, accessible, etc. In addition, TiO<sub>2</sub> photocatalyst has the functions of photoelectric transfer, desideration, sterilization and surface self-cleaning. So, it is used to enhance the environment extensively in the air purification and sewage treatment [1–3]. It exists in three crystalline structures: anatase, rutile and brookite. Anatase and rutile belong to the large bandgap semiconductors with bandgap energies of 3.2 and 3.0 eV, respectively [4]. However, because of its wide forbidden band gap, it excites the electron from valance band to conduction band by UV light, which is available only 4 – 5 % in the solar light. Co-doping of transition metals into the TiO<sub>2</sub> lattice enhances the photocatalytic action by reducing the bandgap in between VB and CB [5]. An appended benefit of transition metal doping like Mn, Cr, Ni, Cu is to improve the trapping of electron to inhibit the e<sup>+</sup>/h<sup>–</sup> recombination during irradiation of light [6, 7]. “Transition metal doped TiO<sub>2</sub> nanoparticles demonstrated that Ni or Mn doped TiO<sub>2</sub> possess better absorption ability of visible light and Ni/Mn either substitutes Ti<sup>4+</sup> site or embeds in the vacancy of TiO<sub>2</sub> lattice” [8].

In the present investigation, among all the transition metals manganese and nickel were selected for the synthesis of Mn–Ni co-doped TiO<sub>2</sub> using the sol-gel method. These metals are preferred because the presence of the *t*<sub>2g</sub> orbital of *d* is very close to the conduction band of TiO<sub>2</sub> by which the absorption is shifted to visible region [9, 10]. Manganese has the greatest potential in permitting significant optical absorption in the visible region through the combined effects of a narrow bandgap and the introduction of intermediate bands within forbidden gap [9]. In the Mn–Ni co-doped TiO<sub>2</sub>, Mn<sup>2+</sup> and Ni<sup>2+</sup> ions replaced the Ti<sup>4+</sup> in TiO<sub>2</sub> lattice because ionic radii of Ti<sup>4+</sup> (0.068 nm) is similar to that of Mn<sup>2+</sup> (0.078 nm) and Ni<sup>2+</sup> (0.072 nm) [11]. On the other hand, the introduction of Ni ions into the TiO<sub>2</sub> lattice can form heterojunctions between n-type TiO<sub>2</sub> and p-type Ni oxide dopant. The presence of p-n junctions can promote the segregation of electron-hole pairs through the electric junction field and facilitate the interfacial charge transfer [12]. There are numerous methods for producing titania nanoparticles, such as sol-gel process, electrochemical coating, hydrothermal process, flame aerosol

process, micro emulsion method, thermolysis, chemical vapor deposition, etc. [13]. Among all these methods, the sol-gel method is often employed and it offers advantages such as precise control over the stoichiometry, low temperature synthesis, high crystallinity and high purity [14].

In the present work, metal ion (Ni, Mn) doped TiO<sub>2</sub> samples were prepared by calcination and their antibacterial activity was studied by measuring zone of inhibition for gram negative pathogens like *Sphingomonas paucimobilis* and *Pseudomonas fluorescense*. *Sphingomonas paucimobilis* (MTCC-6363) has a single polar flagellum with slow motility. It is usually found in soil and water, hospitals and various types of clinical specimens, including respiratory therapy items, humidifiers, water, air, bedside water bottles, sinks, and temperature probes. This organism causes blood stream infections, leg ulcers, and urinary tract infections in humans [15]. *Pseudomonas fluorescense* (MTCC-1688) constitutes large domain of prokaryotic microorganisms. Typically, a few micrometers in length, the bacteria have a number of shapes, ranging from spheres to rods and spirals. *Pseudomonas fluorescense* flourishes in hospital environments and is a particular problem in this environment, since it is the second-most common infection in hospitalized patients [16].

## 2. Experimental

### 2.1. Materials

All the chemicals used in the synthesis process were reagent grade and used without further purification. n-butyl tetra orthotitanate (Ti(OBu)<sub>4</sub>), manganese nitrate ([Mn(NO<sub>3</sub>)<sub>2</sub>].6H<sub>2</sub>O) and nickel nitrate ([Ni(NO<sub>3</sub>)<sub>2</sub>].6H<sub>2</sub>O) were obtained from E-Merck, Germany and used as a precursors for titanium, manganese and nickel for preparing undoped TiO<sub>2</sub> and co-doped TiO<sub>2</sub> catalysts respectively.

### 2.2. Synthesis of nanocatalyst

Manganese and nickel co-doped nanotitania was synthesized by the sol-gel method [17, 18]. In this process, n-butyl tetra orthotitanate (20 mL) was added to 40 mL of ethanol and acidified with 3.2 mL of nitric acid (concentrated HNO<sub>3</sub>) taken in a 150 mL pyrex glass beaker (solution-A) and stirred for 15 min. In another beaker, the required weight (as per the dopant weight percentage) of Mn and Ni from its precursors with respect to titania were taken and added 40 mL of ethanol and then 7.2 mL of deionized water for hydrolysis (solution-B). Then solution-B was added to solution-A drop wise under vigorous stirring. After complete addition of solution-B, a colloidal suspension formed and was stirred continuously for 90 min and aged for 48 h. The obtained gel was dried in an oven at 70 °C, ground in a mortar and calcined at 450 °C for about 5 h in a muffle furnace. Finally, it was cooled and ground to an homogeneous powder. Following the above procedure, different Mn & Ni co-doped catalysts were prepared by varying weight percentages of Mn & Ni (0.25 – 1.0 Wt %) as shown in Table 1. For preparation of undoped TiO<sub>2</sub>, the above procedure is followed without addition of nickel and manganese precursors.

TABLE 1. Name assigned to different weight percentages of co-doped TiO<sub>2</sub> catalyst samples

S. No	Dopant (Transition metal) weight percentages in TiO <sub>2</sub> (Wt %)	Name assigned to co-doped TiO <sub>2</sub> Catalyst
1	1.00 Mn 0.25 Ni	NMT1
2	0.25 Mn 1.00 Ni	NMT2
3	0.50 Mn 0.50 Ni	NMT3
4	0.25 Mn 0.75 Ni	NMT4
5	0.75 Mn 0.25 Ni	NMT5
6	Nil	undoped TiO <sub>2</sub>

### 2.3. Experimental techniques used for characterization of the catalysts

The crystalline structure of photocatalysts were determined by powder X-ray diffraction (XRD) spectra taken (PAN Analytical) using anode Cu-WL 1 ( $\lambda = 1.5406$  nm) radiation with a nickel filter. The applied current and voltage were 40 mA and 40 kV respectively. The average crystallite size of anatase was determined according to the Scherrer equation using full width at half maximum (FWHM) data of the selected peak. The surface area and porosity measurements were carried out with a micrometrics, Gemini VII surface area analyzer. The nitrogen adsorption/desorption isotherms were recorded 2 – 3 times to obtain reproducible results and reported by BJH surface/volume mesopore analysis. The micro pore volume was calculated using the Frenkel–Halsey–Hill isotherm equation. Each sample was degassed at 300 °C for 2 h. The size and shape of the catalyst were recorded with TEM using JEOL/JEM 2100, operated at 200 kV. The morphology and elemental composition of the catalyst were characterized using scanning electron microscope (SEM)

(ZEISS-SUPRA 55 VP) equipped with an energy dispersive X-ray (EDX) spectrophotometer and operated at 20 kV. FT-IR analyses were performed on a FT-IR spectrometer (Nicolet Avatar360). The Diffuse reflectance spectra (DRS) of the catalyst samples were recorded with a Shimadzu 3600 UV-Visible-DRS Spectrophotometer equipped with an integrating sphere diffuse reflectance accessory, using BaSO<sub>4</sub> as reference scatter. Powder samples were loaded into a quartz cell and spectra were recorded in the range of 200 – 900 nm.

#### 2.4. Experimental set up for the antibacterial activity study of photocatalyst

Antibacterial activity study of NMT-2 was carried out by the agar-well diffusion method [19] against bacterial strain namely *Sphingomonas paucimobilis* and *Pseudomonas fluorescence* of Gram-negative pathogens. The nutrient agar (High media – India) dissolved in water was distributed in 100 mL conical flask and sterilized in autoclave at 121 °C 15 lbp for 15 min. After autoclaving, the media was poured into sterilized petri plates which were then swabbed by using L-shaped glass rod with 100 μL of 24 h mature broth of the bacterial strain culture. The wells were made sterile by cork-borer. Wells are created in two different petri plates in the first plate undoped TiO<sub>2</sub> another plates NMT-2 sample solution injected (100, 300 and 400 μg/mL) into the wells. The TiO<sub>2</sub> nanoparticles were dispersed in sterile water and it was used as a negative control and simultaneously the standard antibiotic chloramphenicol (100 μg/mL) as positive control were tested against the bacterial pathogen, then the plates were incubated 24 h at 37 °C. The zone inhibition of every well measured in millimeters.

### 3. Results and discussion

#### 3.1. X-ray diffraction studies (XRD)

Figure 1 shows crystallinity and structural properties of manganese and nickel co-doped TiO<sub>2</sub> of different phases in the XRD patterns of the samples obtained after calcination at 450 °C. All diffraction lines are relatively strong, which indicating a high crystallinity for all samples. Further, the peak positions and relative intensities of the diffraction lines match with standard diffraction data for different TiO<sub>2</sub> phases, i.e. anatase and rutile for NMT1, NMT2, NMT3. The anatase phase was confirmed with the Joint Committee on Powder Diffraction Standard (JCPDS) file no. 21-1272. The peaks at  $2\theta = 25.28, 37.81, \text{ and } 48.05$  corresponded to the (101), (004), and (200) planes of anatase, while the peaks at  $2\theta = 27.29, 44.10 \text{ and } 54.32$ , corresponded to the (110), (101) and (220) planes of rutile structure with the JCPDS file no. 21-1276. The existence of rutile in the nanomaterial was readily discernible from its (110) diffraction peak located at  $2\theta$  of  $27.29^\circ$  in the XRD pattern, because no overlapping of this peak with any other peaks from anatase occurred. Anatase phase can also be easily identified from its (101) peak located at  $2\theta$  of  $25.3^\circ$ , as this peak doesn't overlap with any other peaks of rutile. This result clearly demonstrates that rutile and anatase coexisted in the samples NMT1 – NMT3. The percentage ratio of anatase/rutile was found to be 86:14 estimated using Rietveld refinement method. Further, the samples NMT4, NMT5 and undoped TiO<sub>2</sub> shows anatase phase only. The X-ray diffraction patterns of anatase TiO<sub>2</sub> nanoparticles exhibited broad peaks, indicating small sizes of the nanoparticles at 450 °C calcination temperature while the sharp peaks indicated large nanoparticle sizes. The average crystallite sizes of the samples were determined by the Debye–Scherrer equation using high intensity of anatase (101) and rutile (110) diffraction peaks, the results were shown in Table 2. The XRD patterns of the samples exhibited similar diffraction peaks, indicating that the obtained samples were the TiO<sub>2</sub> nanomaterial consisting of anatase and rutile nanoparticles.

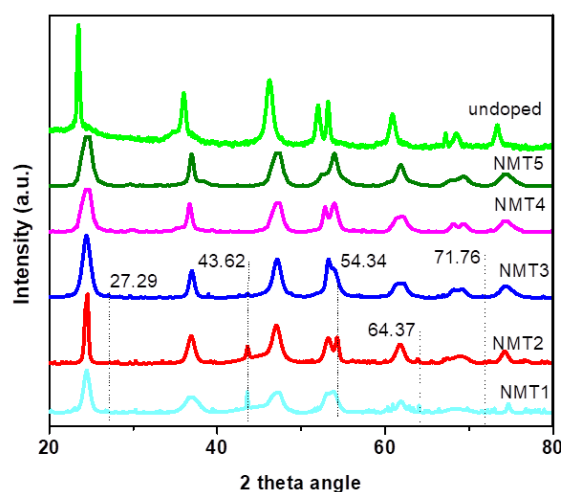


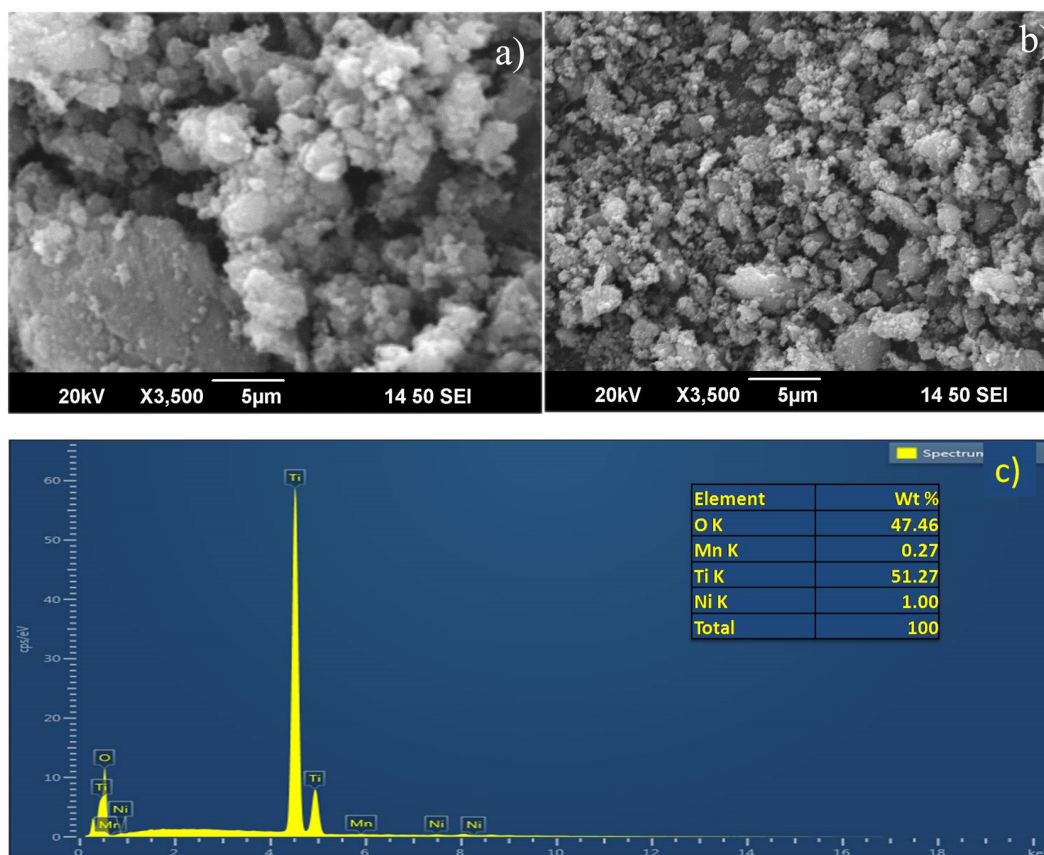
FIG. 1. XRD patterns of undoped and co-doped NMT catalysts

TABLE 2. The results of crystallite size (XRD), band gap (UV-Vis-DRS) and BET surface area

S.No	Catalyst	Crystallite size (nm)	Band gap energy (eV)	BET surface area analysis		
				Surface area (m <sup>2</sup> /g)	Pore volume (cm <sup>3</sup> /g)	Pore size (nm)
1	NMT1	7.35	2.74	113.41	0.22	7.3
2	NMT2	6.5	2.70	135.70	0.22	6.2
3	NMT3	7.31	2.78	114.06	0.22	7.3
4	NMT4	7.9	2.84	106.81	0.20	8.2
5	NMT5	8.50	3.0	88.87	0.20	9.3
6	undoped	18.3	3.20	64.09	0.21	10

### 3.2. Scanning electron microscopy & Energy dispersive spectroscopy (SEM-EDX)

The morphology and particle size of the catalyst, which play very important roles in its photocatalytic activity [20], were examined by the SEM. Fig. 2 shows that the SEM micrograph of the as prepared undoped TiO<sub>2</sub> and NMT2 nanocatalysts. In the Fig. 2(a) undoped TiO<sub>2</sub> clearly revealed large particle size and Fig. 2(b) co-doped TiO<sub>2</sub> shows small particle size, which leads to high surface area, well correlated with BET results. The morphology has different shapes of grains with irregular boundaries. Images of undoped TiO<sub>2</sub> (Fig. 2(a)) show randomly shaped and aggregated particles. HRSEM of 1.00 wt% of Ni and 0.25 wt% of Mn–TiO<sub>2</sub> (Fig. 2(b)) shows irregular tiny clusters composed of large numbers of nanoparticles with lower aggregation and better distribution. From the SEM images it can be inferred that aggregation is decreased greatly due to co-doping. The elemental composition of the prepared catalyst determined by the EDX detector was attached to a SEM shown in Fig. 2(c). EDX analysis revealed that the presence of Ti, O, Ni and Mn elements. No impurities related to precursor molecules were detected.

FIG. 2. SEM images of a) undoped TiO<sub>2</sub> and b) NMT2; c) EDX spectra of NMT2

### 3.3. Transmission electron microscopy (TEM)

The particle size distribution was obtained by measuring the diameter of particles from representative TEM images. The TEM micrographs of undoped and co-doped (NMT2) TiO<sub>2</sub> samples are shown in Fig. 3(a) and (b). From the images it is noticed that the particle size of NMT2 is smaller compared to undoped TiO<sub>2</sub>. The Fig. 3(c) shows the catalyst particles lattice fringes with *d* spacing 0.33 nm corresponding to 101 plane of anatase TiO<sub>2</sub>. The diffraction rings are observed (Fig. 3(d)) for co-doped (NMT2) TiO<sub>2</sub> catalyst from SAED pattern clearly reveals that no structural change of anatase TiO<sub>2</sub> was found; the planes are (101), (004), (200) and (211). Fig. 3(e) shows that the average size of the prepared nanoparticle is 6.5 nm, which was calculated from the Gaussian fitting of the size Histogram [20, 21]. These results confirmed that the co-doping of Ni and Mn reduces the particle size of TiO<sub>2</sub>.

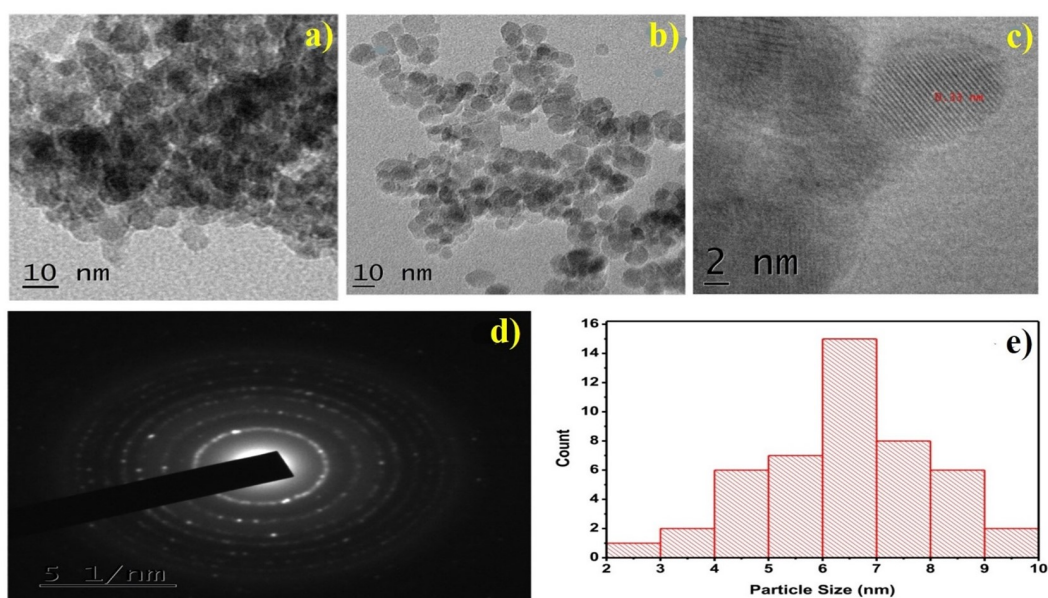


FIG. 3. TEM images of a) undoped TiO<sub>2</sub>; b) NMT2; c) NMT2 showing lattice fringes; d) SAED pattern of NMT2; e) NMT2 particle size distribution

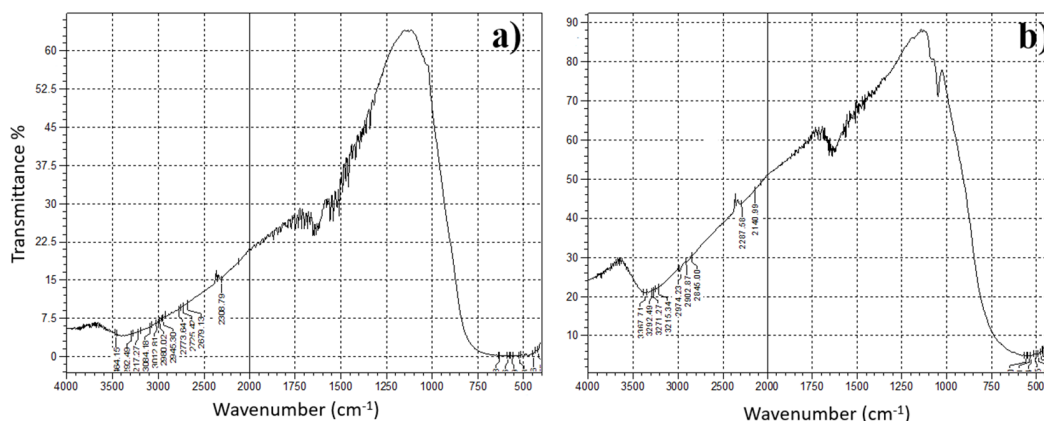
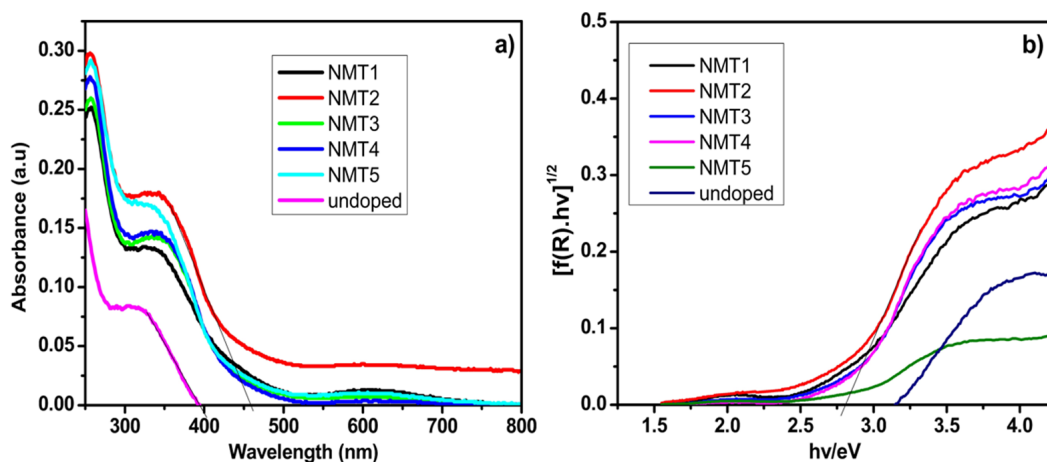
### 3.4. Fourier Transform – Infra Red Spectroscopy (FT-IR)

Undoped and Ni<sup>2+</sup>, Mn<sup>2+</sup> co-doped TiO<sub>2</sub> nanomaterials were identified by FT-IR spectra and were given in Fig. 4. The bands appeared around at 3012, 3464, and 1620 – 1635 cm<sup>-1</sup> [22] corresponding to stretching vibrations of OH belongs to Ti–OH on the surface and bending vibrations of adsorbed H–OH molecule. The strong absorption band around 569 cm<sup>-1</sup> is due to stretching vibrations of Ti–O–Ti and Ti–O band in undoped TiO<sub>2</sub> which is in good agreement with previous studies [23]. From Fig. 4(b) it is seen that after co-doping of Ni and Mn into TiO<sub>2</sub> lattice the stretching vibrations of skeletal Ti–O–Ti shifted to 569 to 605 cm<sup>-1</sup> indicating that Ni and Mn had been co-doped into the TiO<sub>2</sub> lattice by substituting titanium [24]. Further, the increased band intensity located at 1020 cm<sup>-1</sup> for co-doped TiO<sub>2</sub> indicated that Ni and Mn are co-doped into TiO<sub>2</sub> lattice.

### 3.5. Ultraviolet-visible diffuse reflectance spectroscopic studies (UV-Vis-DRS)

The diffused reflectance spectra (DRS) of undoped and Ni, Mn co-doped TiO<sub>2</sub> samples shown in Fig. 5 indicate that the absorption of the electromagnetic spectrum appeared at the visible region (~ 400 – 800 nm). NMTs (Ni and Mn co-doped samples) showed remarkable decreases in band gap and extension of absorption edge towards visible light wavelength (red shift). This is may be due to the formation of an extra energy level above the valance band by Ni 2p leading to narrowing the band gap of TiO<sub>2</sub> [25]. This shift is associated with the doping as well as the formation of stable rutile phase of TiO<sub>2</sub> as illustrated in XRD. The inherent reason for the red shift in the band gap is due to the change of the sp-d exchange interactions between the band electrons and the localized d-electrons of the Ni<sup>2+</sup> ions [26].

The manganese ions incorporated into TiO<sub>2</sub> lattice distort the surrounding environment which affects the conduction band of TiO<sub>2</sub> through the interaction with Ti-3d orbitals which helps to suppress the recombination of electron hole pairs and extended the optical response [27]. Furthermore, this was supported by the calculated band gap energies of all the synthesized samples from the reflectance spectra using the Kubelka–Monk formalism and Tauc plot method [28] shown in Fig. 5(b). The undoped TiO<sub>2</sub> exhibited a band gap of 3.2 eV, which is comparable with the literature value [29] and the co-doped TiO<sub>2</sub> sample showing the band gap ranging from 2.7 to 3.01 eV. Among all the co-doped samples, NMT2 exhibited the lowest band gap energy (2.70 eV). Thus, the results indicated that all the co-doped samples are visible light-active and enhance the photocatalytic degradation efficiency due to the formation of more number of photo generated


 FIG. 4. FT-IR spectra of a) undoped TiO<sub>2</sub>; b) NMT2

 FIG. 5. (a) The DRS spectra of undoped and co-doped TiO<sub>2</sub> with different Wt% of Mn and Ni; (b) Tauc plots of the square root of the Kubelka–Munk function determining band gap energy values

electron/hole pairs. Further, when compared the band gap values of Mn and Ni single doped TiO<sub>2</sub> catalysts (which are obtained from literature value), the band gap of NMT2 catalyst is reduced and the values are given in Table 3 [30, 31].

 TABLE 3. The comparative band gap values of Mn and Ni single doped and Mn and Ni co-doped TiO<sub>2</sub>

S.No	Doping elements	Catalysts band gap energy (eV)	Reference No.
1	Mn	2.95	28
2	Ni	2.99	29
3	Undoped TiO <sub>2</sub>	3.2	27
4	Mn and Ni	2.70	Present work

### 3.6. Brauner–Emmett–Teller (BET)

The specific surface area and porosity of the undoped TiO<sub>2</sub> and NMT2 were investigated by using the N<sub>2</sub> adsorption and desorption isotherms as shown in Fig. 6(a). All the isotherms of samples revealed the stepwise adsorption and desorption branch of type IV curves, indicating the presence of mesoporous material having a three-dimensional (3D) intersection according to IUPAC classification. A hysteresis loop with a stepwise adsorption and desorption branch is observed at wide range of pressure ( $P/P_0$ ), and the surface area of NMT2 mesoporous TiO<sub>2</sub> calcined at 450 °C is 135.70 m<sup>2</sup>/g as shown in Fig. 6(a). The undoped TiO<sub>2</sub> surface area is 64 m<sup>2</sup>/g as shown in Fig. 6(a). This result indicates that the synthesized material has wider mesoporous structure. To analyze pore size and pore volume, the plots of the pore size distribution are investigated by desorption branch of the BJH method as shown in Fig. 6(b). The average pore

diameter of mesoporous  $\text{TiO}_2$  calcined at  $450^\circ\text{C}$  is 6.2 nm with relatively narrow pore size distribution. The pore volume of mesoporous  $\text{TiO}_2$  is  $0.22\text{ cm}^3/\text{g}$ . However, for undoped  $\text{TiO}_2$ , a 10 nm pore size distribution is observed and  $0.21\text{ cm}^3/\text{g}$  pore volume is also counted. Such physical properties of large surface area and high crystallinity with nano crystalline aggregated make a material a good candidate for high photocatalytic activity. This increased surface area may favor the adsorption of the more number of dye molecules on the surface of the catalyst, which enhances the degradation efficiency of the catalyst.

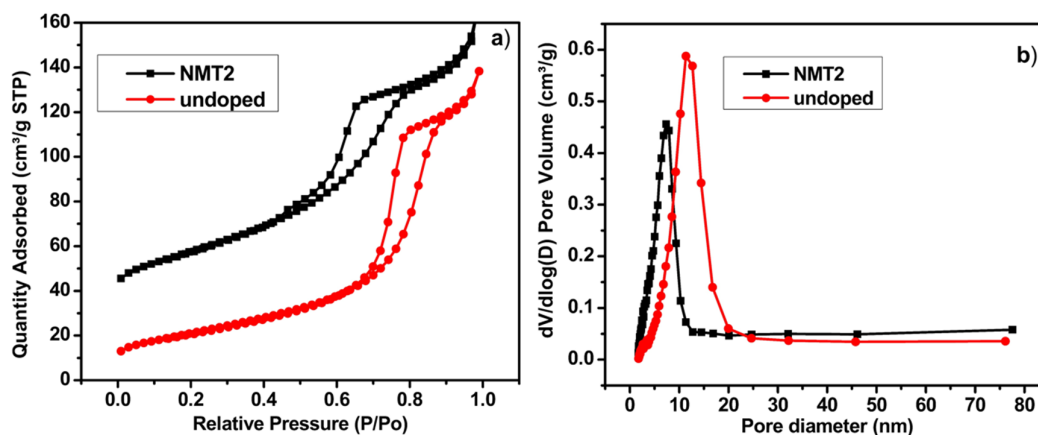


FIG. 6. (a) The  $\text{N}_2$  adsorption–desorption isotherms and (b) pore diameter distribution curves of NMT2 co-doped  $\text{TiO}_2$

#### 4. Evaluation of antibacterial activity of Ni and Mn co-doped $\text{TiO}_2$ on *Sphingomonas paucimobilis* and *Pseudomonas fluorescense*

##### 4.1. Antibacterial activity of NMT2 catalyst against *Sphingomonas paucimobilis*

The antibacterial activity of co-doped  $\text{TiO}_2$  nanoparticles were carried out by the agar-well diffusion method against *Sphingomonas paucimobilis* (MTCC-6363) at different concentrations of undoped and co-doped  $\text{TiO}_2$  (NMT2) nanoparticles ranging from 100, 300, 400  $\mu\text{g}/\text{mL}$  and control (chloramphenicol – 100  $\mu\text{g}/\text{mL}$ ). Performance standards for antimicrobial susceptibility tests were conducted [32]. The antibacterial petri plates are shown in Fig. 7(a) – undoped  $\text{TiO}_2$  and Fig. 7(b) – co-doped  $\text{TiO}_2$ .  $\text{TiO}_2$  petri plates showed the bacterial growth zone diameters; and from those, the results are presented in Table 4. From the table, the value represented the zone of inhibition of bacterial growth for *Sphingomonas paucimobilis* at 400  $\mu\text{g}/\text{mL}$  was  $25.1 \pm 0.2\text{ mm}$ . These results showed that 400  $\mu\text{g}/\text{mL}$  is the best concentration for the zone of inhibition of bacterial growth compared with standard reference (chloramphenicol) and undoped  $\text{TiO}_2$ . Further, we have calculated T-test values for three replicates of each bacterium by using SPSS software and the values are given in Table 5.

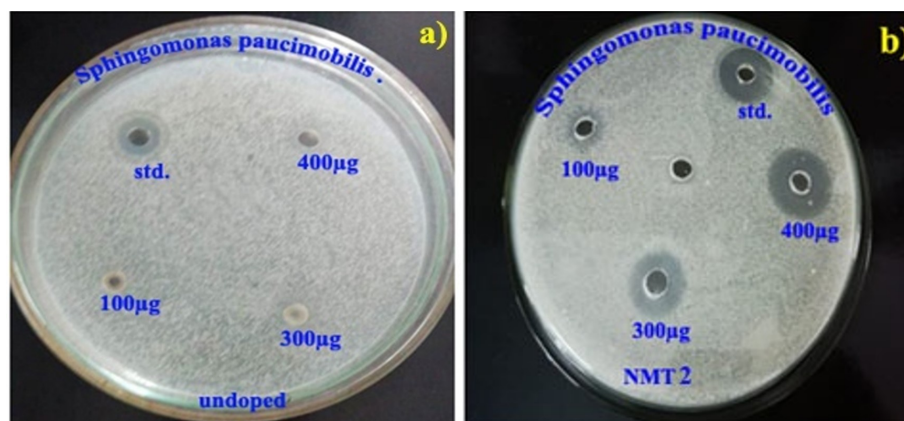


FIG. 7. Zone of inhibition of *Sphingomonas paucimobilis* by (a) Undoped  $\text{TiO}_2$  and (b) NMT2 Catalyst

TABLE 4. Agar-well diffusion of undoped and co-doped TiO<sub>2</sub> nanoparticles (NMT2) on *Sphingomonas paucimobilis* (MTCC-6363)

S.No	Catalyst	Organism	Zone of inhibition (mm)			
			100 µg/mL	300 µg/mL	400 µg/mL	Standard (Chloramphenicol) 100 µg/mL
1	(NMT-2)	<i>Sphingomonas paucimobilis</i> (MTCC-6363)	14.3 ± 0.25	20.2 ± 0.26	25.1 ± 0.2	24.1 ± 0.1
2	Undoped TiO <sub>2</sub>	<i>Sphingomonas paucimobilis</i> (MTCC-6363)	—	—	—	24.1 ± 0.1

TABLE 5. Determination of mean of three replicates for zone of inhibition of *Sphingomonas paucimobilis*(MTCC-6363) with NMT2 nanocatalyst

Parameter	100 µg/mL	300 µg/mL	400 µg/mL	100 µg/mL (Standard)
Mean	14.30	19.03	25.90	24.1
SD	0.25	0.25	0.15	0.05
T-test	96.71	70.25	151.81*	434.74
P value	0.00	0.00	0.00	0.00

Mean of three replicates ± Standard deviation

\*P < 0.05 was consider as significant difference

**4.2. Antibacterial activity of NMT2 catalyst on *Pseudomonas fluorescens* (MTCC-1688)**

The antibacterial activity of co-doped TiO<sub>2</sub> nanoparticles were carried out by the agar-well diffusion method against *Pseudomonas fluorescens* (MTCC-1688) at different concentrations of undoped and co-doped TiO<sub>2</sub> (NMT2) nanoparticles ranging from 100, 300, 400 µg/mL and control (chloramphenicol – 100 µg/mL). The antibacterial petri plates are shown in Fig. 8(a) – undoped TiO<sub>2</sub> and Fig. 8(b) – co-doped TiO<sub>2</sub>. As before, the TiO<sub>2</sub> petri plates showed the bacterial growth zone diameters, and the results are presented in Table 6. In this table, the values represented the zone of inhibition of bacterial growth for *Pseudomonas fluorescens* (MTCC-1688). At 400 µg/mL, this value was 18.1 ± 0.2 mm. These results showed that 400 µg/mL was the best concentration for the zone of inhibition of bacterial growth compared with standard (chloramphenicol) and undoped TiO<sub>2</sub>. Further, we have calculated T-test values for three replicates of each bacterium by using SPSS software and the values are given in Table 7. This zone of inhibition of bacterial growth with the catalyst may be due to exposure of catalyst with the visible light formation of e<sup>-</sup>/h<sup>+</sup> pairs which can acts as a strong oxidizing agent and the excited electron can reacts with adsorbed oxygen and converted to reactive oxygen species (e.g., super oxide radicals which in turns produces OH). Then these e<sup>-</sup>/h<sup>+</sup> and OH both can be acts as oxidizing agents which can degrade the protein coat of bacteria, leading to the inhibition of the growth of the organism during the catalysis.

TABLE 6. Agar-well diffusion of undoped and co-doped TiO<sub>2</sub> nanoparticles (NMT2) on *Pseudomonas fluorescens* (MTCC-1688)

S. No	Catalyst	Organism	Zone of inhibition (mm) (Mean of three replicates ± SD)			
			100 µg/mL	300 µg/mL	400 µg/mL	Standard (Chloramphenicol) 100 µg/mL
1	NMT2	<i>Pseudomonas fluorescens</i> (MTCC-1688)	5.8 ± 0.43	12.6 ± 0.25	18.1 ± 0.17	23.1 ± 0.05
2	Undoped TiO <sub>2</sub>	<i>Pseudomonas fluorescens</i> (MTCC-1688)	—	—	—	23.1 ± 0.05

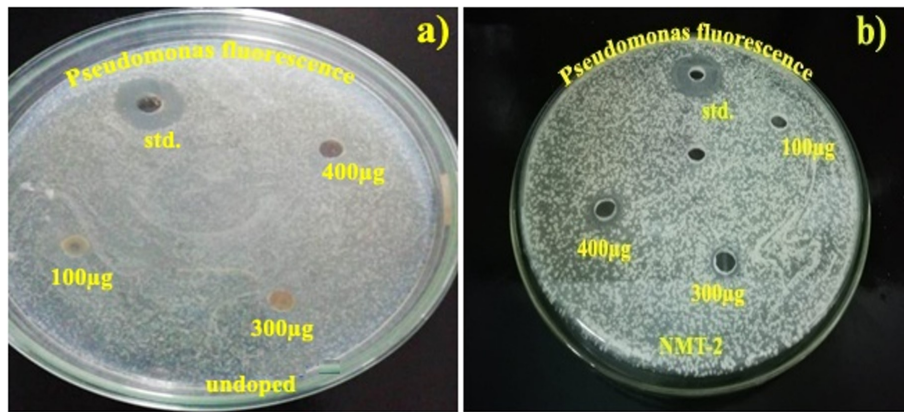


FIG. 8. Zone of inhibition of *Pseudomonas fluorescens* (MTCC-1688) by a) Undoped TiO<sub>2</sub>; b) NMT2 Catalyst

TABLE 7. Determination of mean of three replicates for zone of inhibition of *Pseudomonas fluorescens* (MTCC-1688) with NMT2 nanocatalyst

Parameter	100 µg/mL	300 µg/mL	400 µg/mL	100 µg/mL (Standard)
Mean	5.30	12.03	18.10	23.16
SD	0.25	0.25	0.05	0.05
T-test	96.71	70.25	151.81*	434.74
P value	0.00	0.00	0.00	0.00

Mean of three replicates ± Standard deviation

\* $P < 0.05$  was consider as significant difference

In this case, hydroxyl radicals were released by the photocatalyst when irradiated by visible light. The bactericidal effect of co-doped TiO<sub>2</sub> has generally been attributed to the decomposition of bacterial outer membranes by reactive oxygen species (ROS), primarily hydroxyl radicals (OH), which leads to phospholipid peroxidation and ultimately cell death. Hence the generated hydroxyl radicals acted as powerful oxidizing agents which may be reacting with peptidoglycan (poly-N-acetylglucoseamine and N-acetylmuramic acid) of the bacterial outer cell wall. This promotes the disruption of cell respiration leading to the destruction of bacteria.

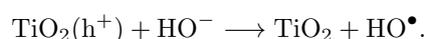
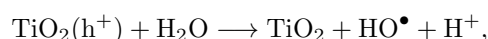
#### 4.3. Photocatalytic mechanism for photodegradation of bacteria

The reactive catalyst particles play a key role in the production of hydroxyl radicals (HO<sup>•</sup>) leading to antibacterial activity. The photocatalytic mechanism by co-doped TiO<sub>2</sub> is briefly represented as follows.

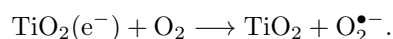
The following steps are the prime steps for formation of <sup>•</sup>OH. Its formation is an important step in the photocatalytic degradation of pollutants and the antibacterial activity of photocatalyst. When co-doped TiO<sub>2</sub> nano powder is irradiated with visible light, the electrons are excited to the conduction band, leaving behind the holes in the valence band. The recombination of the generated electrons and holes must be prevented for effective utilization of the catalyst. Thus, generated electrons are captured by the doped dopant ions preventing their recombination:



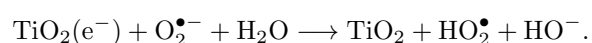
The holes react with surface bound hydroxyl groups or with water adsorbed on the surface of TiO<sub>2</sub> to produce hydroxyl radicals and hydrogen ions:



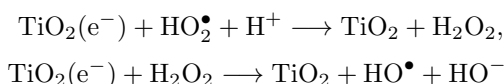
The electrons are transferred to adsorbed oxygen producing superoxide anion:



These superoxide anions further react with adsorbed water molecules producing peroxide radicals and hydroxyl ions:



The peroxide radicals combine with H<sup>+</sup> resulting in the formation of hydroxyl radicals and hydroxyl ions. Hydrogen peroxide is formed as an intermediate product:



Holes oxidize these hydroxyl ions to hydroxyl radicals. Thus, all the species facilitate the formation of HO<sup>•</sup>. The strong oxidizing HO<sup>•</sup> reacts with the outer part peptidoglycan of bacteria and degrade it.



Thus, the formation of hydroxyl radicals and their role in photocatalytic activity plays an essential role in the degradation mechanism.

## 5. Conclusions

In the current work, nanocatalysts are synthesized by sol-gel method and these are calcined at 450 °C. These samples are characterized by various techniques. Co-doping of transition metal into TiO<sub>2</sub> lattice ceases the electron-hole recombination and reduces the bandgap. Moreover, co-doped TiO<sub>2</sub> nanomaterials exhibit excellent antibacterial performance. The XRD results reveals that the anatase and rutile mixed phase was observed for the co-doped samples. FTIR stretching frequencies confirmed the shifting of absorption band of TiO<sub>2</sub> from UV to visible region. SEM-EDS shows morphology and composition of the photocatalyst. UV-vis-DRS, TEM and BET reported bandgap, particle size and surface area respectively. These photocatalytically active materials antibacterial activities were deduced by using *Sphingomonas paucimobilis* and *Pseudomonas fluorescense*. The results show that among all the nanocatalysts, NMT2 catalyst shows optimum zone of inhibition at 25.1 ± 0.2 mm for *Sphingomonas paucimobilis* and 18.1 ± 0.2 mm for *Pseudomonas fluorescense* compared to standard (chloramphenicol) value at 24.1 ± 0.1 mm and 23.1 ± 0.05 mm at 100 µg/mL respectively.

## References

- [1] Fujishima A., Kobayakawa K., Honda K. Electrochemical photolysis of water at a semiconductor electrode. *Nature*, 1972, **238**, P. 37–38.
- [2] Mital G.S., Tripathi M. A review on the synthesis of TiO<sub>2</sub> nanoparticles by solution route. *Central European J. of Chemistry*, 2021, **10** (2), P. 279–294.
- [3] Fujishima A., Rao T.N., Tryle D. Titanium Dioxide photocatalysis. *J. of photochemistry and photobiology C: photochemistry reviews*, 2000, **1**, P. 1–21.
- [4] Vassilios B., Danae V., Dimitrios K., George K. Modified TiO<sub>2</sub> based photocatalysts for improved air and health quality. *J. of Materiomics*, 2017, **3** (1), P. 3–16.
- [5] Ashahi R., Morikawa T. Visible–light photocatalysis in Nitrogen-doped Titanium oxides. *Science*, 2001, **293**, P. 269–271.
- [6] Umar K., Aris A., et al. Synthesis of visible light active doped TiO<sub>2</sub> for the degradation of organic pollutants—methylene blue and glyphosate. *J. of Analytical Science and Technology*, 2016, **7**, 29.
- [7] Jing D., Zhang Y., Guo L. Study on the synthesis of Ni doped mesoporous TiO<sub>2</sub> and its photocatalytic activity for hydrogen evolution in aqueous methanol solution. *Chemical Physics Letters*, 2005, **415**, P. 74–78.
- [8] Muditana S.R., Tirukkovalluri S.R., Alim A.S., Imandi M.R. Photocatalytic degradation of allura red by Mn–Ni co-doped nanotitania under visible light irradiation. *IJITEE*, 2019, **8**, P. 650–657.
- [9] Zhao C.F., Song L., et al. Electronic, optical and photocatalytic behavior of Mn, N doped and codoped TiO<sub>2</sub>: Experiment and simulation. *J. of Solid State Chemistry*, 2016, **235**, P. 160–168.
- [10] Pelaez M., Nicholas T.N., et al. A review on the visible light active titanium dioxide photocatalysts for environmental applications. *Applied Catalysis B: Environmental*, 2012, **125**, P. 331–349.
- [11] Shifu C., Sujuani Z., Wei W.Z. Preparation and activity evaluation of p–n junction photocatalyst NiO/TiO<sub>2</sub>. *J. of Hazardous Materials*, 2008, **55**, P. 320–326.
- [12] Wilke K., Breuer H.D. The influence of transition metal doping on the physical and photocatalytic properties of titania. *J. of Photochemistry and Photobiology A: Chemistry*, 1999, **121**, P. 49–53.
- [13] Tavakoli A., Sohrabi M., Kargariandii Ali. A Review of Methods for Synthesis of Nanostructured Metals with Emphasis on Iron Compounds. *Chemical Papers*, 2007, **61**, P. 151–170.
- [14] Rafiq M.A., Ikram M., Nafees M., Ali S. Structural, optical and magnetic study of Nidoped TiO<sub>2</sub> nanoparticles synthesized by solgel method. *Int. Nano Letters*, 2018, **8**, P. 1–8.
- [15] Boyan B., James H., Judicael P. Principles of assessing bacterial susceptibility to antibiotics using the agar diffusion method. *J. of Antimicrobial Chemotherapy*, 2008, **61** (6), 1295.
- [16] Cappucino J.G., Sherman N. Microbiology, A Laboratory Manual. 6th Ed., Pearson Education (Singapore) Ltd, 2004, **4**, 199.
- [17] Avasarala B.K., Raori T.S., Sridher B. Enhanced photocatalytic activity of beryllium doped titania in visible light on the degradation of methyl orange dye. *Int. J. of Materials Research*, 2010, **101**, P. 1–7.
- [18] Alim S.A., Rao T.S., et al. Fabrication of visible light driven nano structured Copper, Boron codoped TiO<sub>2</sub> for photocatalytic removal of Lissamine Green B. *J. of Saudi Chemical Societies*, 2019, **23**, P. 92–103.
- [19] Liu G., Wang K., Zhou Z. Influence of doping on antibacterial effect of TiO<sub>2</sub> nanoparticles. *Materials Science Forum*, 2006, **510–511**, P. 86–89.
- [20] Gharibshahi E., Saion E. Influence of dose on particle size and optical properties of colloidal platinum nanoparticles. *Int. J. of Molecular Sciences*, 2012, **13**, P. 14723–14741.
- [21] Taranjeeti K., Abhishek S., Amrit P.T. Wanchoo R.K. Utilization of solar energy for the degradation of carbendazim and propiconazole Fe doped TiO<sub>2</sub>. *Solari Energy*, 2016, **125**, P. 65–76.
- [22] Zhongping Y., Fanghou J., et al. Microporous Ni-doped TiO<sub>2</sub> film photocatalyst by plasma electrolytic oxidation. *Applied Materials Science*, 2010, **2**, P. 2617–2622.

- [23] Sharotri N., Sud D. Aigreener approach to synthesize visible light responsive nanoporous S-doped TiO<sub>2</sub> with enhanced photocatalytic activity. *New J. of Chemistry*, 2015, **39**, P. 217–223.
- [24] Othmana I., Mohamed R. Ibrahim F. Study of photocatalytic oxidation of indigo carmine dye on Mn supported TiO<sub>2</sub>. *J. of Photochemistry and Photobiology A: Chemistry*, 2007, **189**, P. 80–85.
- [25] Jensen S., Kilin S.D. Electronic properties of Ni-doped TiO<sub>2</sub> anatase. *J. of Physics: Condensed Matter*, 2015, **27**, P. 1–13.
- [26] Shah S.M., Hussain S.M.H. Effect of carrier concentration on the optical band gap of TiO<sub>2</sub> nanoparticles. *Materials & Design*, 2016, **96**, P. 64–72.
- [27] Wang Y., Zhang R., Liangliang J., Lin L.S. First principles study on transition metal-doped anatase TiO<sub>2</sub>. *Nanoscale Research Letters*, 2014, **9**, P. 35–46.
- [28] Chang S., Chien-yao H., Pin-haniand L., Chang T. Preparation of phosphate Zr doped TiO<sub>2</sub> exhibiting high photocatalytic activity through calcination of ligand-capped nanocrystals. *Applied Catalysis B: Environmental*, 2009, **90**, P. 233–241.
- [29] Christian D., Osorio S.M.P., et al. TiO<sub>2</sub> anatase with a bandgap in the visible region. *Nano Letters*, 2014, **14**, P. 6533–6538.
- [30] Chauhan R., Kumar R., Chaudhary A.P. Structural and photocatalytic studies of Mn doped TiO<sub>2</sub> nanoparticles. *Spectrochimica Acta Part A: Molecular and Biomolecular Spectroscopy*, 2012, **98**, P. 256–264.
- [31] Bhatia V., Dhir A. Transition metal doped TiO<sub>2</sub> mediated photocatalytic degradation of anti-inflammatory drug under solar irradiations. *J. of Environmental Chemical Engineering*, 2016, **4**, P. 1267–1273.
- [32] Jayaseelan C., Rahuman A.A., et al. Biological approach to synthesize TiO<sub>2</sub> nanoparticles using aeromonas hydrophilia and its antibacterial activity. *Spectrochimica Acta Part A: Molecular and Biomolecular Spectroscopy*, 2013, **107**, P. 82–89.

---

Submitted 13 June 2021; revised 15 November 2021; accepted 30 December 2021

*Information about the authors:*

Sankara Rao Muditana – Department of Chemistry, Government Degree College, Puttur, Chittoor, Andhra Pradesh – 517583, India; Department of Inorganic & Analytical Chemistry, A.U. College of Science & Technology, Andhra University, Visakhapatnam, Andhra Pradesh – 530003, India; ORCID 0000-0001-7988-9022; sraom90@gmail.com

Siva Rao Tirukkovalluri – Department of Inorganic & Analytical Chemistry, A.U. College of Science & Technology, Andhra University, Visakhapatnam, Andhra Pradesh – 530003, India; ORCID 0000-0001-5156-1885; sivaraoau@gmail.com

Imandi Manga Raju – Department of Inorganic & Analytical Chemistry, A.U. College of Science & Technology, Andhra University, Visakhapatnam, Andhra Pradesh – 530003, India; ORCID 0000-0002-6291-601X; mangorchem@gmail.com

*Conflict of interest:* the authors declare no conflict of interest.